Red Supergiants, Yellow Hypergiants, and Post-RSG Evolution

Michael S. Gordon [1,*,†] and **Roberta M. Humphreys** [2]

[1] SOFIA Science Center, NASA Ames Research Center, Mountain View, CA 94035-0001, USA
[2] Minnesota Institute for Astrophysics, School of Physics and Astronomy, 116 Church St. SE, University of Minnesota, Minneapolis, MN 55455, USA; roberta@umn.edu
[*] Correspondence: mgordon@sofia.usra.edu
[†] Current address: SOFIA Science Center, NASA Ames Research Center, Moffett Field, CA 940353, USA.

Abstract: How massive stars end their lives remains an open question in the field of star evolution. While the majority of stars above $\gtrsim 9$ M$_\odot$ will become red supergiants (RSGs), the terminal state of these massive stars can be heavily influenced by their mass-loss histories. Periods of enhanced circumstellar wind activity can drive stars off the RSG branch of the HR Diagram. This phase, known as post-RSG evolution, may well be tied to high mass-loss events or eruptions as seen in the Luminous Blue Variables (LBVs) and other massive stars. This article highlights some of the recent observational and modeling studies that seek to characterize this unique class of stars, the post-RSGs and link them to other massive objects on the HR Diagram such as LBVs, Yellow Hypergiants and dusty RSGs.

Keywords: evolved stars; Yellow Hypergiants; Red Supergiants; stellar mass loss

1. Introduction

The standard model of massive star evolution follows a rapid progression from the main-sequence, through a blue supergiant (BSG) phase, to the red supergiant (RSG) branch, to terminal supernova (SN) explosion. However, surveys of the brightest supergiants revealed an empirical upper luminosity limit to stars on the Hertzsprung-Russell (HR) diagram [1]. This limit suggests that stars above some initial zero-age main-sequence (ZAMS) mass ($\approx$30–40 M$_\odot$) do not evolve to the RSG branch on the HR Diagram and therefore follow an alternative evolutionary pathway. Since the 1980s, both observational and modeling studies have attempted to describe and constrain the stellar populations and instabilities at the upper luminosity boundary, as well as explore the local environments that influence these massive stars during both their main- and post-main-sequence lives.

It has long been established that massive stars at any stage of evolution provide a favorable environment for enhanced mass-loss in their stellar winds due to low surface gravity (g) in their outer atmospheres. The outer circumstellar (CS) material is only tenuously gravitationally bound to the star itself. Indeed, mass-loss rates for RSGs range from 10^{-6} M$_\odot$ yr^{-1} [2,3] to as high as 10^{-4} M$_\odot$ yr^{-1} in extreme supergiant stars like VY CMa [4]—mass-loss rates that represent a significant fraction of a star's initial mass being shed during its post-main-sequence lifetime. The evolution and terminal state of a massive star is ultimately governed not just by its ZAMS mass but also by these drastic changes in total stellar mass and outer envelope conditions. We refer to these changes in stellar mass through ejection of CS material as the "mass-loss history." In this chapter, we summarize some of the literature on the mass-loss histories of evolved supergiant stars and the evidence for post-red supergiant evolution both in observational studies of the circumstellar ejecta and in evolutionary models that predict the effect of various mass-loss mechanisms on massive star evolution.

2. Context—The Red Supergiant Problem

Further context for much of the observational exploration of the last decade comes from a recently-identified "red supergiant problem" [5–7]. A survey of Type II-P supernova progenitors using optical and near-IR pre-explosion archival images revealed an upper limit of only 16–17 $M_\odot$ for the initial stellar masses of their likely red supergiant (RSG) progenitors [6]. Type II-P SN remnants are a useful laboratory for population statistics of RSGs since they represent the most abundant class of CCSNe (∼70% of hydrogen-rich SNe; see [8] for a discussion of SN rate estimates).

From the notable lack of II-P SN progenitors above ∼17 $M_\odot$ (Figure 1), Smartt et al. [6] suggested two possible scenarios:

1. Systematic underestimation of progenitor mass due to improper extinction correction.
2. Red supergiants greater than 17 $M_\odot$ have another terminal state besides II-P CCSNe.

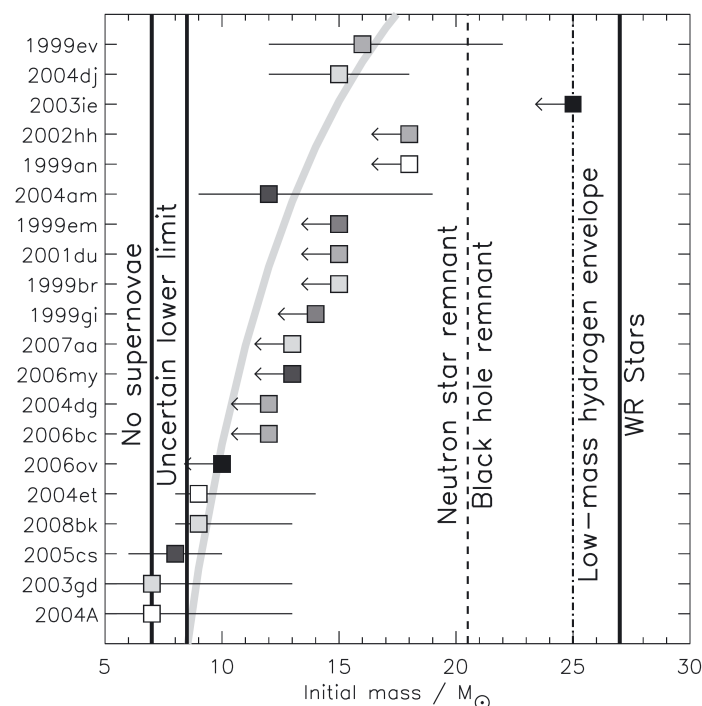We explore these two scenarios below.

Figure 1. Initial masses of observed supernova (SN) Type II-P progenitors in the Smartt et al. [6] survey. Labels indicate theoretical limits for types of compact remnants. Darker shading is higher metallicity. The thick gray line represents a cumulative frequency distribution of a Salpeter IMF with $\Gamma = -1.35$. Figure reproduced from Smartt et al. [6].

Though no Type II-P SN progenitors appear to exist much above ∼16 $M_\odot$, red supergiants have certainly been observed with masses far greater than this. For examples, see the recent HR Diagrams for massive evolved stars in the Galaxy [9], the Magellanic Clouds [10] and in M31 and M33 [11–13] A comparison with the evolutionary models [14], illustrates that many stars are present on the RSG branch above 20 $M_\odot$ in Local Group galaxies.

One potential caveat for these RSG surveys is that the derived masses require accurate measurement of bolometric luminosity. As Smartt et al. [6] suggest in scenario 1. above, underestimating RSG masses could be a potential solution to the RSG problem. Extra intrinsic extinction due to dust close to the RSG progenitor would yield lower luminosities and their estimated masses [15,16]. Indeed, mass-loss rates and dust ejecta masses scale with luminosity [3,13,17]. Additionally, mid-IR interferometry around evolved stars has revealed dust close enough in to the central source [18] that the dust grains could potentially be destroyed by the star's SN explosion.

Walmswell and Eldridge [16] examined the effect of dust on derived RSG masses by applying the Cambridge STARS code [19,20] combined with various mass-loss schema [21–23] to simulate SEDs throughout a massive star's evolution. They model a series of dust shells and estimate a simulated extinction to measure an average A_V of around 1 mag from the circumstellar ejecta. The resulting model SEDs do indeed yield lower deduced stellar masses than what would have been observed with proper extinction-correction for the model dust shells, with an underestimate of as much as 5 $M_\odot$ for supergiants in the $\sim 20-25\,M_\odot$ range. Still, the authors note that even a change in several solar masses worth of dust material does not solve the red supergiant problem.

Beasor and Davies [24] explored this missing mass problem combining mid-IR WISE and Spitzer/IRAC photometry with circumstellar dust shell models from DUSTY [25]. The authors apply their model analysis to a co-eval population of RSG cluster stars (NGC 2100), which allows for studying stars with similar initial conditions—mass, metallicity, local environment and so forth. If the cluster stars all have roughly the same initial masses (within a few tenths of a solar mass), then the evolutionary pathway should be the same and any differences in luminosity should be due to the slightly more massive stars evolving faster on the HR Diagram. This allowed the authors to use luminosity as a proxy for evolution. Based on their models and estimated mass-loss rates, they find an increase in mass-loss rates along the RSG branch as high as a factor of 40 over the post-main-sequence lifetime of the star, which appears to be consistent with the de Jager et al. [21] mass-loss prescription. If the increased mass loss is translated into an intrinsic extinction, they argue that the increased reddening may substantially increase derived masses of Type II-P SN RSG progenitors. As an example, the authors show that similar dust extinction conditions on SNe 1999gi, 2001du and 2012ec could revise initial mass estimates by as many as 10 $M_\odot$.

Kilpatrick and Foley [26], however, argue that while circumstellar dust can alter the observed SEDs of supergiant progenitors, several studies of the circumstellar environments around SN progenitors suggest that there cannot be enough material around at least some SN Type II progenitor systems to hide an underlying high-mass RSG. They note that the total dust mass in progenitor systems is independently constrained by radio and X-ray observations. For example, X-ray light curves of CCSNe have been used to estimate stellar wind parameters and the density structure of the CS medium [27,28]. Many of these studies, though, have broad wavelength coverage of the SN progenitor SED. It is possible that for some RSG progenitors with less constrained SEDs and sparse pre-SN imaging/photometry, the "missing mass" scenario from CS dust may indeed be biasing RSG mass statistics. However, as IR photometry exists for many SN RSG progenitors, this argument is only a partial solution to the red supergiant problem.

As for scenario 2. above from Smartt et al. [6]—that high-mass red supergiant progenitors simply do not exist—there are two possible explanations: first, that higher mass RSGs collapse directly to black holes; and second, that stellar evolution to the warmer, blue side of the HR Diagram produces stellar end products other than Type II-P SNe. The subject of black hole formation, either through direct collapse or fall back, merits a longer discussion that is beyond the scope of this work. For a review of some of the work surrounding black hole formation in massive stars, see the annual review by Smartt [29].

One realm of exploration in the literature is the idea of failed supernovae, or "unnova"—stars that collapse to black holes with little or no energy released (e.g., References [30–33]). Such events may have no significant transient and thus may be almost impossible to observe [34]. However, models by Lovegrove and Woosley [35] and Piro [36] find that RSGs in the 15–25 $M_\odot$ range can lose so much energy in neutrinos during collapse that the resulting shock in the stellar envelope is expected to create an optical signature. This can be as bright as $L_{\rm bol} \sim 10^6 - 10^7\,L_\odot$, though perhaps lasting for only a few days [36].

These results suggest that an optical transient of this type from a failed SN would have only a small observable window, thereby decreasing the likelihood of detection. Nonetheless, surveys like that on the LBT [30,33,37] have potentially found one such source, N6946-BH1, which brightened to $\gtrsim 10^6\,L_\odot$ in March 2009 before fading below its pre-outburst luminosity [33]. SED modeling constrained the mass of the RSG progenitor to $\sim 25\,M_\odot$ [37], above the apparent Smartt et al. [6] SN Type II-P progenitor

limit. Based on near-IR IRAC photometry and an unusually high dust temperature, Humphreys [38] suggests that the progenitor may have actually been a warm hypergiant in a post-RSG state, rather than an M-type RSG. Despite a decade of monitoring, objects like this remain exceedingly rare. While failed SNe may indeed represent some high-mass RSG population that is as of yet undiscovered, for the moment this does not seem to solve missing high-mass SN progenitors.

In this chapter, we focus on another population of transient objects—the yellow supergiants (YSGs) and hypergiants and evidence for post-red supergiant evolution.

3. The Milky Way Hypergiants and Post-RSG Evolution

Many years before attention was drawn to the red supergiant problem, a small group of high luminosity evolved supergiants was recognized with a range of intermediate to cool temperatures, high mass loss and unstable atmospheres (see several papers cited in Reference [39]). These stars, now referred to as yellow or red hypergiants, defined the empirical upper luminosity boundary in the HR Diagram for evolved massive stars [1]. The well-studied members of this elite group are Galactic members with a few examples in the Magellanic Clouds and M31 and M33 (Section 5). The visibly bright Galactic stars all exhibit spectroscopic and photometric variability, high mass loss and several show dusty ejecta. The evolutionary state of the warm or yellow hypergiants was not obvious; they could be evolving toward the red supergiant region or on a blue-loop back to warmer temperatures. The instability and brief high mass-loss events exhibited by ρ Cas, for example, Reference [40], during which it developed TiO bands and the increasing evidence for episodic high mass-loss events especially visible in the ejecta of IRC +10420 (Section 4) favored a post-RSG evolved state for these stars.

Other warm or yellow hypergiants include the Galactic stars HR 8752 and HR 5171A [41–43]. These hypergiants are visually bright and relatively nearby, which has made them important laboratories for study of late-stage evolution. Interestingly, de Jager [44] suggests that all of the yellow hypergiants are post-red supergiants. During blueward evolution, their atmospheres contract, the atmospheric opacity increases and their rotation increases. Having shed a sizable fraction of their mass on the RSG branch, these stars are now closer to the Eddington Limit for their ZAMS mass. The stars thus enter a temperature range (6000–9000 K) of increased dynamical instability, that de Jager called the "yellow void," where high mass-loss episodes occur. Figure 2 is a schematic HR Diagram showing the positions of some of the better-studied Galactic yellow hypergiants plus Var A in M33 with respect to the critical temperature region.
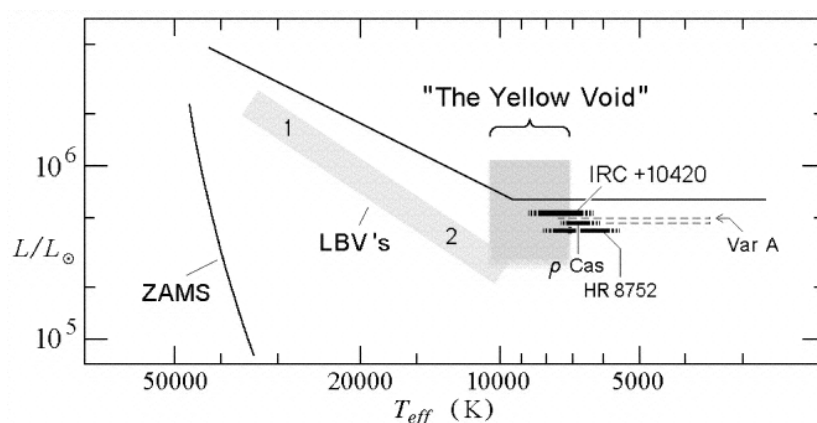

Figure 2. Schematic HRD of Galactic warm hypergiants (and Var A in M33) illustrating the location of these massive stars relative to the Humphreys-Davidson limit [1] and the "yellow void"—a temperature and luminosity band region for increased dynamical instability. The location of the LBV instability strip is also shown with the classical (LBV 1) and less-luminous (LBV 2) LBVs in their quiescent state.

4. IRC +10420 and Var A in M33—Clues to Post-RSG Evolution

The luminosities and apparent temperatures of the two evolved yellow supergiants IRC +10420 and Var A place them at the upper luminosity boundary for evolved stars in the HR Diagram. Both stars exhibit a history of photometric and spectroscopic variability with high mass loss episodes and dusty circumstellar ejecta making them excellent candidates for post-red supergiant evolution.

At its initial discovery, IRC +10420 (V1302 Aql) was quickly recognized as remarkable with its very large infrared excess and late F-type high luminosity spectrum [45]. It was soon identified as a powerful maser source and is one of the warmest known OH/IR stars [46].

IRC +10420 is a Galactic star and because of its relative proximity, its circumstellar ejecta is easily resolved by HST imaging [47] which revealed a complex environment. The color image in Figure 3 shows the spatial extent of the ejecta, more that 5 arcsec across. Numerous features are visible within two arcsec of the embedded star including condensations arrayed in jet-like structures, rays and an intriguing group of small, nearly spherical shells or arcs apparently at the ends of some of the jet-like features. One or more distant reflection shells at 5 to 6 arcsec from the star are visible in the longer exposure images.
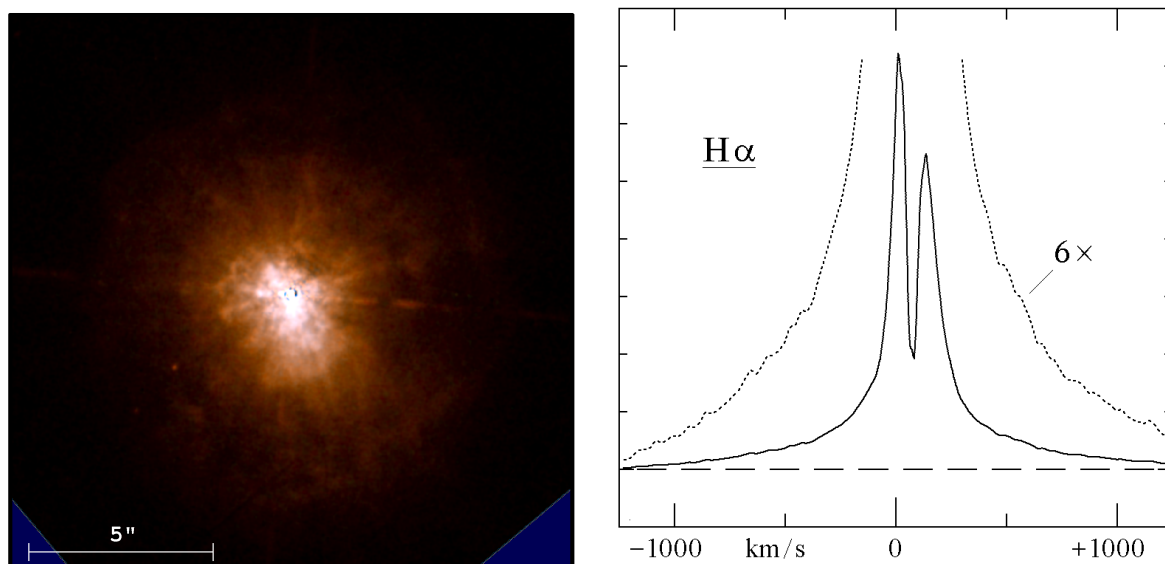

Figure 3. Left: The combined color image of IRC +10420 from HST/WFPC2 [47]. **Right**: Profile of the Hα emission line showing the broad electron scattering wings and the split profile (adapted from Reference [48]).

While its actual distance is somewhat uncertain, numerous arguments (e.g., Reference [49]) clearly demonstrated that it was not a post-AGB star and therefore above the AGB-limit at $M_{Bol} \approx -7$ mag. The reddening of its optical spectral energy distribution, infrared polarization and its radial velocity [50] suggested a distance of 4–6 kpc and a luminosity of $\approx -9.6 \pm 0.5$ mag (at 5 kpc), which places IRC +10420 at the upper luminosity boundary in the HRD for evolved stars. Jones et al. [50] therefore proposed that IRC +10420 may be evolving from a red supergiant across the HR Diagram to warmer temperatures and in a phase of its evolution analogous to the post-AGB lower mass giants evolving to the planetary nebula phase but at much higher luminosities.

The early photographic image-tube spectra [45] showed late F-type absorption features, however, 23 years later, Oudmaijer [51] identified H lines and other absorption features typical of a warmer A-type supergiant implying a significant change in its apparent temperature. HST/STIS spectra a few years later were consistent with the higher temperature [48]. The spectrum is dominated by a strong Hα stellar wind split emission line (Figure 3, right) due either to a bi-polar outflow or an equatorial disk. Strong Ca II triplet emission lines, also with a split profiles and the [Ca II] doublet in emission

formed in the extended low density ejecta plus numerous Fe II emission lines typical of a stellar wind are present. Humphreys et al. [48] demonstrated that the wind was optically thick. Thus, observed variations in the apparent spectral type and the inferred temperature are due to changes in the wind and not to changes in the interior, that is, evolution, of the star on such a short timescale. Subsequent spectroscopic monitoring by Klochkova et al. [52] and by our group do not show any further increase in its apparent temperature suggesting that the blueward motion of IRC +10420 on the HR Diagram has slowed.

The morphology of IRC +10420's circumstellar ejecta had always been elusive, with suggestions of a bipolar outflow or a circumstellar disk with different orientations ranging from edge-on to an inclined disk at different angles. To investigate its three-dimensional morphology, Tiffany et al. [53] combined the transverse velocities for several knots and condensations in the inner ejecta, measured from second-epoch HST imaging, with their Doppler velocities. The resulting total space motions and direction of the outflows showed that these knots were ejected at different times and in different directions over the last $\approx$400 years, a relatively recent period of asymmetric mass loss. Interestingly, they are all moving within a few degrees of the plane of the sky. Thus we are viewing IRC +10420 nearly pole-on and are looking nearly directly down onto its equatorial plane. This orientation is confirmed by both the highly polarized 2.2 μm emission around the star, which places the scattering dust in the plane of the sky [54] and high resolution near-infrared interferometry [55]. The more distant reflection shells were ejected about 3000 years ago, suggesting more than one epoch of high mass loss.

To explore IRC +10420's mass loss history, Shenoy et al. [56] used far-infrared imaging from SOFIA/FORCAST at 11–37 μm to probe the extended cold dust plus high-resolution adaptive optics imaging at 8–12 μm. They found evidence for two distinct periods of high mass loss, an earlier episode from 6000 to about 2000 years ago with a high rate of $2 \times 10^{-3}\,M_\odot\,yr^{-1}$, followed by an order of magnitude decrease with a current rate of $\approx 10^{-4}\,M_\odot\,yr^{-1}$, consistent with other recent measurements. This change is additional evidence for IRC +10420's evolution from the red supergiant stage and its transition to a warmer state.

Var A in M33 is significant since it has actually been observed to transition to a red supergiant and back to its presumably normal state as a high luminosity F-type supergiant within the last century. This color and spectral change, however, was not due to interior evolution but to a high mass-loss episode that produced a dense, cooler wind. Var A provides additional evidence for the highly unstable state of evolved stars near the upper limit in the HR Diagram. This supergiant has the important advantage that its distance and therefore its intrinisic luminosity, $M_{Bol} \approx -9.5$, are known. In M33, however, it is too distant for direct imaging of its ejecta.

Var A is one of the original Hubble-Sandage (H-S) variables [57]. However, unlike the other H-S variables that have been subsequently identified as evolved hot stars with episodes of high mass loss—the LBVs—Var A's quiescent state is a high luminosity yellow or intermediate temperature supergiant. Its historic light curve (Figure 6 in Reference [57]) is remarkable. At maximum light it was one of the visually-brightest stars in M33 but then in 1951 its luminosity rapidly declined by 3.5 mag, becoming faint and red after what had been a slow increase in brightness during the previous 50 years. Spectra from 1985 and 1986 revealed an M-type supergiant with prominent TiO bands [58]. Its spectral energy distribution not only showed the shift to cooler temperatures but a large mid-infrared excess due to extensive circumstellar dust and Var A was as luminous at 10 μm as at its visual maximum. The star had experienced a high mass-loss event that had produced an optically thick, cooler wind—a "false" or "pseudo" photosphere—that resembled a red supergiant.

Subsequent spectra, not observed until 2003–2004, revealed that its "eruption," which had begun ~1951, had indeed ended, having lasted $\approx$45 years [59]. The spectrum showed that the star or its dense wind was now in a much warmer state with absorption lines consistent with an F-type supergiant and emission lines of Ca II, [Ca II] and K I, similar to IRC +10420, in addition to strong H emission formed in it surrounding low-density gas. The optical photometry shows the transition to bluer, warmer colors but Var A remained visually faint and was still obscured by circumstellar dust. The spectra from

1985 and 2004 are shown in Figure 4 and its light curve and SED in Figure 5. Its 10 μm flux shows an unexpected decline, which implies an unexpected decrease in the star's total luminosity. The most likely explanation is that the radiation is escaping in some direction other than our line-of-sight. This possibility is supported by recent spectra of small clumps and knots in the inner ejecta of the red hypergiant VY CMa (Reference [60], see Section 6.1 below), which require a clear line of sight to the star and therefore imply large, low density regions even holes in the circumstellar material which may also be the case for Var A.

Thus, Var A and IRC +10420 are not only probable post-red supergiants but their shared characteristics of photometric and spectroscopic variability, surface instability and stellar winds, high mass loss and a history of enhanced mass-loss episodes are clues to understanding the evolution of stars near the upper luminosity boundary and their transit across the HRD from red to blue.
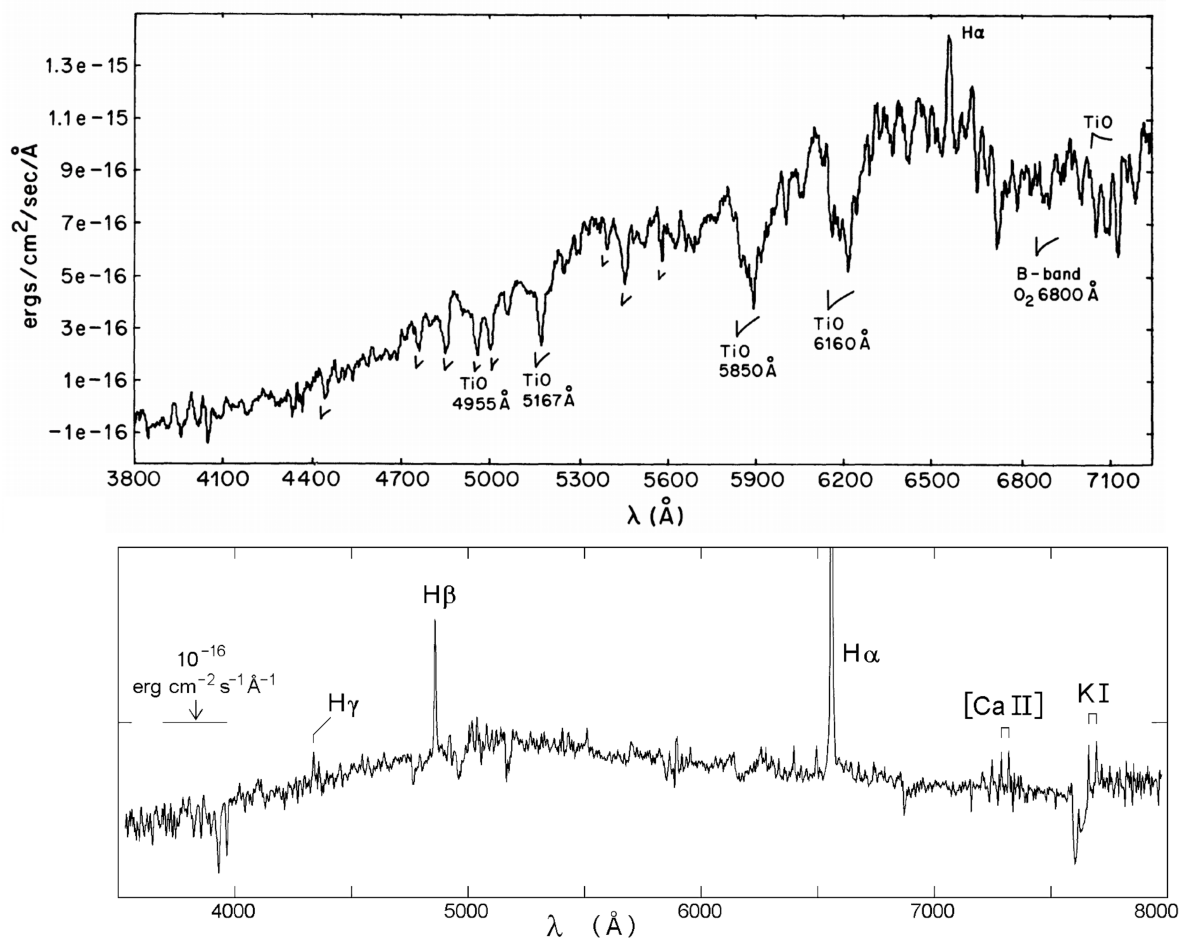

Figure 4. Top: Optical spectrum of Var A from 1985 [58] showing Hα emission and TiO absorption bands. **Bottom**: Optical spectrum of Var A from 2004 [59] with the strongest emission lines marked.
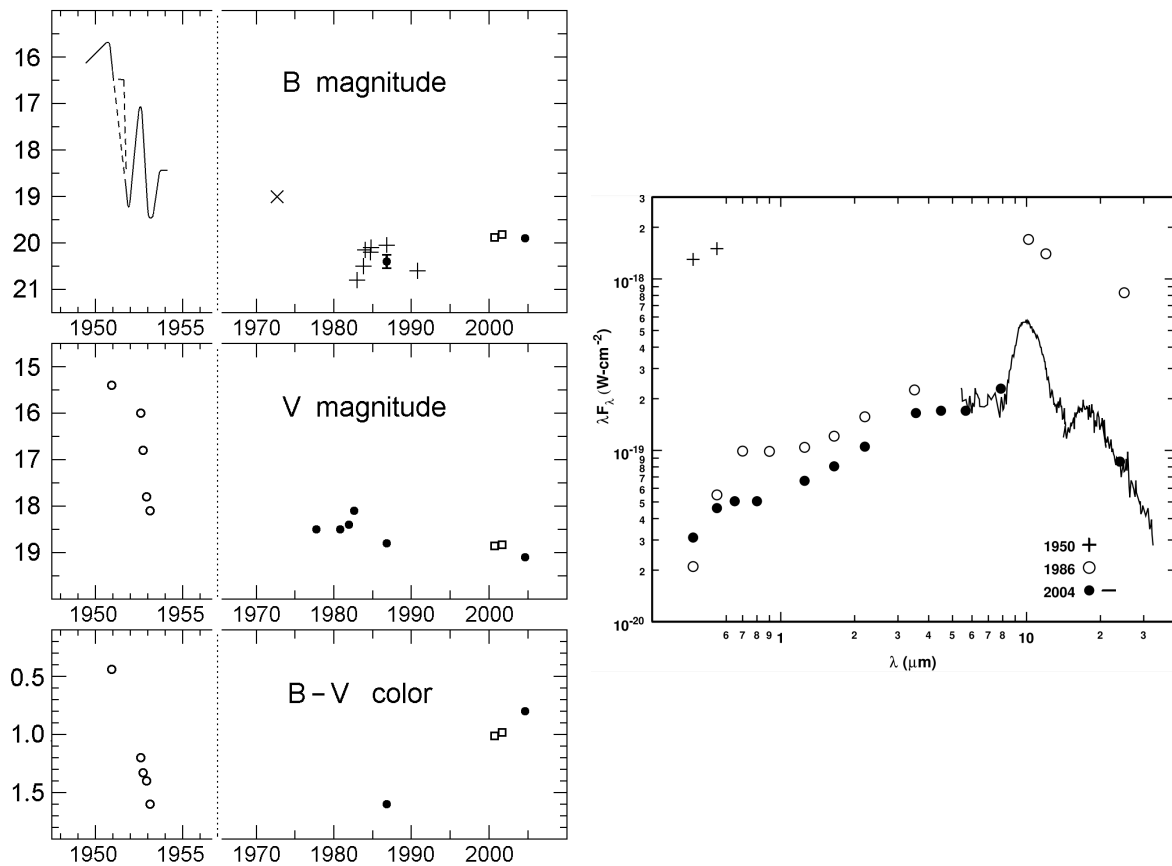
Figure 5. Left: Light curve of Var A from 1950 to the present. The top panel shows the photographic and B-band magnitudes. The middle and bottom panels show the variability in the V-band and the B–V color. See Reference [59]. **Right**: Spectral energy distribution of Var A from 1986 [58,59]. The plus signs show its apparent magnitudes at maximum light from Reference [57].

5. YSGs and Post-RSG Candidates in M31 and M33

Other than Var A, IRC +10420 and the Galactic hypergiant candidates, what fraction of known evolved supergiants may be in a post-RSG state? These statistics, as well as the physical characteristics of candidate post-RSGs and their locations on the HR Diagram, are crucial to our understanding the final stages of the majority of massive stars.

Due in part to their position on the HR Diagram, few post-RSGs are known. They occupy a relatively brief, transient state between the blue and red supergiants and may either be evolving from the main sequence to cooler temperatures, or back to warmer temperatures from the RSG stage. In the Galaxy, the warm or yellow hypergiants, close to the upper luminosity boundary in the HRD with high mass-loss rates, enhanced abundances and dusty CS environments, are excellent candidates for post-RSG evolution. These stars contrast with the intermediate-type yellow supergiants which have normal spectra and long-wavelength SEDs—that is, no evidence for circumstellar dust or mass loss in their spectra. Considering how few objects of this type are known locally, many studies have pursued observations of supergiants outside of the Galaxy.

As part of a larger program on the luminous and variable emission-line stars in M31 and M33, Humphreys et al. [4] recognized a few high luminosity, A- to F-type stars in each galaxy with spectroscopic evidence for high mass loss and extensive gaseous and dusty circumstellar ejecta revealed in their spectra and SEDs; characteristics shared with the warm hypergiants IRC +10420 and the peculiar Var A also in M33. They demonstrated that these stars were indeed evolved, intermediate temperature supergiants with strong winds and mass loss and like IRC +10420 and Var A, they were candidates for post-RSG evolution. Based on their luminosities, their initial masses

would be greater than 20 M$_\odot$ or more. One possible exception was B324, one of the visually brightest stars in M33. Its SED showed strong free-free emission in the near-infrared but lacked the cooler dust expected in a post-RSG star. B324, just at the upper luminosity boundary, with high mass loss, could be approaching the limit to its redward evolution and therefore a candidate for future high mass episodes. Humphreys et al. [4] had identified a few candidates but was not a comprehensive survey for post-red supergiants.

Gordon et al. [13] conducted a survey of the yellow and red supergiants to search for post-RSG candidates. The targets were primarily selected from the published surveys of M31 and M33 for yellow and red supergiants [11,12,61] chosen from the Local Group Galaxies Survey (LGGS; [62]). Post-RSG candidates were identified based on spectroscopic evidence for mass loss and the presence of circumstellar dust in their SEDs. In that work, Gordon et al. [13] spectroscopically confirmed 75 YSGs in M31, 30 of which (40%) are likely in a post-RSG state based on spectroscopic and photometric markers for dusty wind. For M33, 27 of the observed 86 YSGs (31%) were determined to be post-RSG candidates. Further discussion of this work and its methodologies is included below. We note that a similar survey was conducted by Kourniotis et al. [63], which flagged yellow super and hypergiant candidates based on photometric criteria for follow-up spectroscopy.

The greatest challenge in photometric surveys of supergiants is distinguishing extragalactic sources from foreground disk dwarfs as well as halo giants in the Milky Way. Humphreys and Sandage [64] highlighted the magnitude of this issue in a survey of the brightest blue and red supergiants in M33. There is significant contamination of foreground K and M dwarfs in the red supergiant region of the M33 color-magnitude diagram (CMD), which presents some observational challenges. Since there is little star formation in the Milky Way halo, there is essentially no foreground contamination in the "blue plume" of the CMD. Massey et al. [65] applied the Bahcall and Soneira [66] model to estimate that almost 80% of red stars ($1.2 < B - V < 1.8$) fainter than $V \sim 16$ seen toward M31 will be foreground stars. The central portion of the CMD, representing the yellow supergiant population, is similarly affected by foreground contamination. Drout et al. [61] and later Massey et al. [67] apply the Besançon model [68] of the Milky Way (two disks + halo) to illustrate that over 70% of bright stars redward of the blue plume ($B - V > 0.4$) could be foreground contamination.

Massey et al. [11], Massey [69] and Drout et al. [12] demonstrated that color criteria could be used as an effective metric for distinguishing foreground contaminants in the RSG surveys in M31 and M33 but few such two-color discriminants have been used for YSGs, except for Bonanos et al. [70,71], who defined color ranges for a variety of massive star types in the Magellanic Clouds using 2MASS and Spitzer/IRAC photometry. In general, however, spectra are needed to determine both extragalactic membership and evolutionary state.

5.1. Spectral Types and Luminosity Classification

Drout et al. [12,61] use radial velocities from spectral-line features to generate a catalog of extragalactic YSG candidates, whereas both Gordon et al. [13] and Massey et al. [67] classified the stars based on the spectral type and luminosity criteria in their absorption-line spectra. For example, the blends of Ti II and Fe II at $\lambda\lambda$4172-8 and $\lambda\lambda$4395-4400 are valuable luminosity criteria in the blue when compared against Fe I lines, which show little luminosity sensitivity such as λ4046 and λ4271. The O I λ7774 triplet in the red spectra—also used in Drout et al. [12] as part of their classification scheme—is also a particularly strong luminosity indicator in A- to F-type supergiants.

Using these and several other classifiers, Gordon et al. [13] confirmed extragalactic membership of $\sim$150 yellow supergiants in M31 and M33. Thirty, or $\sim$20%, of the observed YSGs in each galaxy showed evidence for stellar winds in their ejecta and enhanced mass-loss, not shared with the other YSGs and therefore possible post-RSG evolution. The notable spectral features include P Cygni profiles in hydrogen emission, broad wings in Hα or Hβ emission indicative of Thomson scattering and [Ca II]/Ca II triplet emission from circumstellar gas. If mass-loss markers in the YSG SEDs are

included (discussed below), the fraction of YSGs likely in a post-RSG state increases to ∼40% of the observed sources.

5.2. Photometric Evidence of Mass Loss

Gordon et al. [13] also examined the SEDs of the YSG and RSG populations in M31 and M33 to identify what fraction of the evolved supergiants have circumstellar dust and are in a mass-losing state. The RSGs currently experiencing episodes of high mass loss may eventually evolve to become post-RSG warm supergiants, LBVs, or WR stars.

The defining signature of mass loss in RSGs is the presence of circumstellar dust, usually revealed as excess radiation in their IR SEDs from the silicate emission features at 9.8 μm and 18 μm, corresponding to the Si–O vibrational [72] and O–Si–O bending modes [73], respectively. The strength of the silicate emission feature is (to first order) correlated with the luminosity and apparent temperature as revealed by the spectral type; that is, the higher the luminosity and cooler the star, the stronger the silicate emission and the larger the IR excess, as well as a larger mass of ejected dust.

In the YSGs, the presence of excess radiation due to circumstellar warm dust and/or free-free emission in the near and mid-infrared wavelengths is evidence for mass loss. This additional radiation is apparent in their SEDs if the flux in the near-IR bands exceeds the expected Rayleigh-Jeans tail of the stellar component. For example, an infrared excess in the 1–2 μm 2MASS bands is a well-known characteristic of free-free emission in stellar winds, while the 3.6 to 8 μm Spitzer/IRAC data provides evidence for warm CS dust. Free-free emission is generally identified as constant F_ν in the near-infrared, often extending out to 5 μm. Examples are shown in Figure 6 for two warm hypergiants in M31. Beyond being useful for identifying mass loss, this IR excess in the stellar SED is crucial for accurately calculating the bolometric luminosity. The CS dust will re-radiate the central star's optical flux into the infrared and this processed radiation can contribute significantly to the total bolometric luminosity of the star + ejecta system. There are various methods for fitting models to stellar SEDs to account for this and an example can be found in Kourniotis et al. [63], who fit an ATLAS9 stellar atmosphere model [74,75] for the stellar component and up to three distinct blackbodies for the warm and cool dust components of their YSG SEDs.

Gordon et al. [13] find ∼50–60% of the observed RSGs in M31 and M33 show evidence for an IR excess in their near- to mid-IR SEDs. The IRAC 8 μm photometry is used in Gordon et al. [13] to provide an estimate of the total dust mass lost over a timescale of about a century and estimate that the RSGs in both galaxies tend to have dusty ejecta of the order of 10^{-3}–10^{-2} M$_\odot$, assuming a warm dust component of ∼350 K. Consistent with the de Jager et al. [21] prescription, mass loss correlates with luminosity along the RSG branch. If more than 50% of RSGs are indeed experiencing sufficient mass loss to produce CS dusty ejecta, a large fraction of stars along the RSG branch may evolve back toward the blue to become the warm post-RSG stars before their terminal state as SNe or black holes.

We note that the target selection from Gordon et al. [13] was derived from optical surveys. Thus, it may be likely that our surveys of the most luminous stars in M31 and M33 do not necessarily include some supergiant populations that are heavily obscured. Since the most luminous warm and cool supergiant populations are likely to have the highest mass-loss rates, it is probable that some will be obscured in the optical by their own CS ejecta in the optical surveys. To complete the upper portion of the HRD would require a further search in the IR to find the brightest infrared sources. There are several IR surveys of M31 and M33 with Spitzer/IRAC (References [76–78], for example) that have specifically targeted the bright and/or variable stellar populations in the Local Group. These surveys have already revealed many unique supergiant stars that were obscured in high-resolution optical surveys—for example, the discovery of optically-obscured η Carinae analogs by Khan et al. [79].
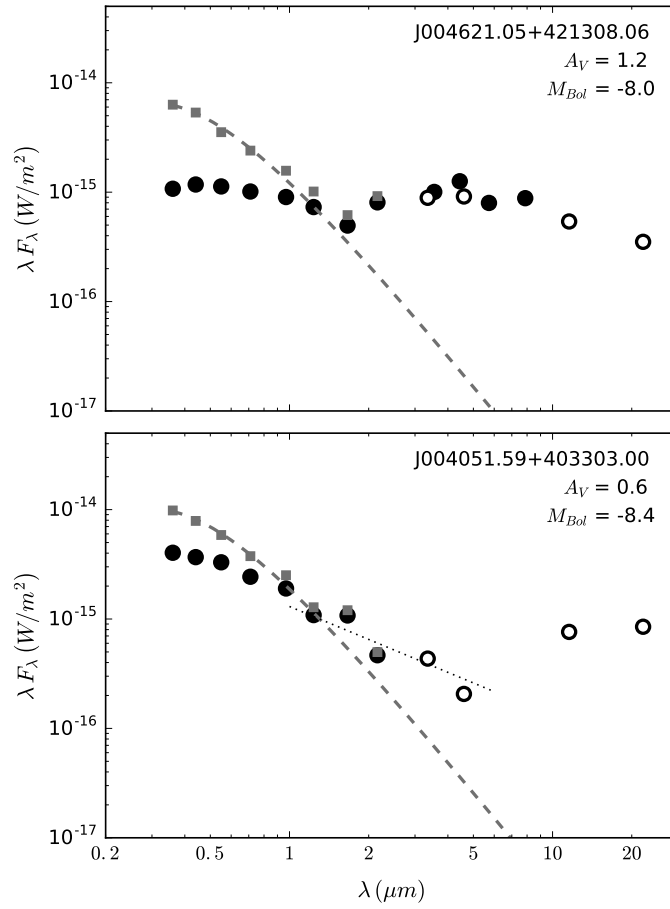
Figure 6. SEDs of warm hypergiant candidates in M31. The observed visual, 2MASS and IRAC magnitudes are shown as filled circles and WISE data as open circles. The extinction-corrected photometry is plotted as filled squares, with the measured line-of-sight A_V specified in each legend. The SED of J004621.05+421308.06 (**top**) reveals a prominent CS dust envelope in the IRAC and WISE bands. The WISE photometry of J004051.59+403303.00 (**bottom**) is suggestive of silicate dust emission but is most likely due to contamination from a nearby H II region and nebulosity. The dotted line is a curve of constant F_ν, which is evidence for free-free emission in wind. Figure adapted from Reference [13].

5.3. The Post-RSG Candidates, the HR Diagram and Comparison with Evolutionary Models

The HR Diagrams for the observed YSGs and RSGs in M31 and M33 Gordon et al. [13] are reproduced in Figure 7. For the YSGs with observed optical spectra, effective temperatures can be derived through comparison to intrinsic colors of the stars' identified spectral types. However, for sources without observed spectra/spectral-type, several photometric temperature scales exist in the literature. For example, Massey et al. [11] compare the $(V - K)$ colors of their M31 RSGs to MARCS atmosphere synthetic photometric colors and Drout et al. [12] adopt the $(V - R)$ color transformations from LMC sources [10] for their observed RSGs in M33. We note that in the absence of spectral types, photometric temperature scales can be somewhat uncertain.

In both M31 and M33, the post-RSG candidates—flagged in Gordon et al. [13] based on their spectroscopic and/or photometric mass-loss indicators—are preferentially more abundant at higher luminosities. Also shown in Figure 7 are Geneva Group [80,81] evolutionary tracks for different ZAMS mass models. The higher mass models (M $\gtrsim 20\,M_\odot$) loop through the YSG region of the HRD, perhaps even in multiple passes, before terminating on the RSG branch. These stars are those supergiants undergoing post-RSG evolution and are sometimes referred to in the literature as "group

2 blue supergiants", (e.g, References [82,83]). We loosely define the YSG region as ∼4000 to 12,000 K and this evolution across the HRD can occur over timescales of just a few Myr.
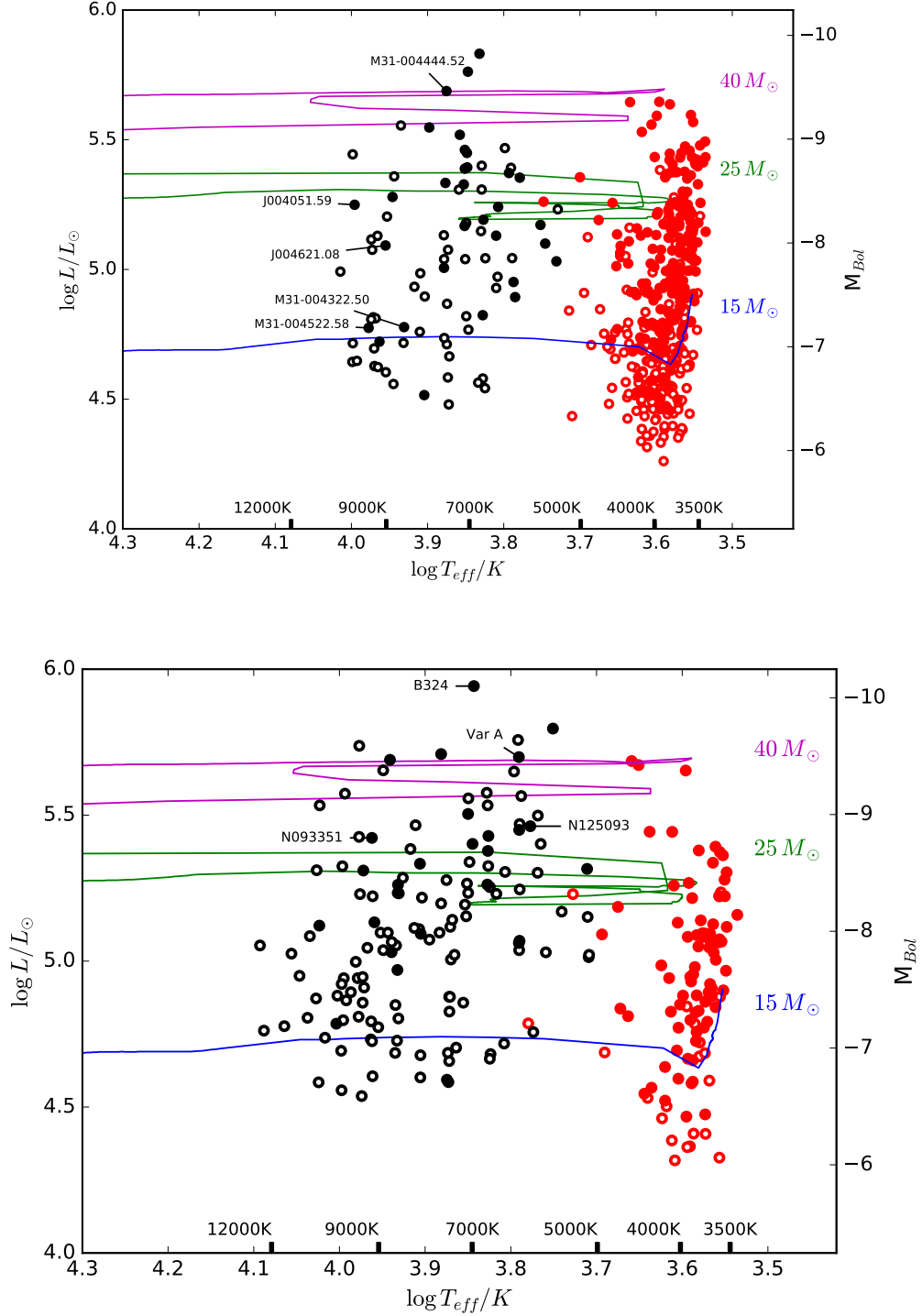

Figure 7. HR Diagrams of M31 (**top**) and M33 (**bottom**). Red circles represent the RSG sample from Gordon et al. [13], black circles are the YSGs. Closed symbols are sources with evidence of mass loss, either in their spectra (for the YSGs) or their SEDs (for both the YSGs and RSGs). Non-rotating stellar evolution tracks for three mass bins from Ekström et al. [80] are shown for comparison. The stars with mass loss, the post-RSG candidates, appear to dominate the upper portion of the HR diagram. Figures adapted from Reference [13].

Comparison with the evolutionary tracks suggests that most of the progenitor main-sequence stars have masses $\gtrsim 20 \, M_\odot$. Likewise, the dusty RSGs dominate the higher luminosities. This is not surprising considering results from Mauron and Josselin [3] (Figure 8) and others that $\dot{M}$ and total mass lost in the RSGs correlates with luminosity.

HR Diagrams of massive stars in the Local Group like those in Gordon et al. [13] and others, such as References [10–12,63,67,84,85], suggest that the mass-losing post-RSG candidates are more common at luminosities above $\sim 10^5 \, L_\odot$. Most appear to have initial masses of 20–40 $M_\odot$ and may be the evolutionary descendants of the more massive RSGs that do not explode as supernovae (i.e., the "missing" RSGs from Smartt et al. [6]). The eventual fate of these stars may be either as "less-luminous" LBVs or WR stars before their terminal explosion.

6. Mass-Loss in the Yellow and Red Supergiants

For many YSG and RSG stars, the thermal excess flux is fairly constant across the mid-infrared, which implies that the dust is emitting over a range of temperatures and distances from the central star. With some assumptions on dust temperature, grain size distributions, silicate grain chemistry and gas-to-dust ratio, near- to mid-infrared photometry can be used directly to estimate the total mass of the CS ejecta around each supergiant star. With some additional measurements and/or assumptions on timescales—such as the stellar wind velocity [4,13] or the dust condensation timescale—estimates on mass-loss rates can be extracted from the mid-infrared flux alone. For example, Mauron and Josselin [3] apply the de Jager et al. [21] mass-loss prescription to Galactic RSGs to estimate an average mass-loss rate of $\sim 10^{-6} \, M_\odot \, yr^{-1}$ from IRAS 60 µm flux. Figure 8 from Mauron and Josselin [3] illustrates the de Jager et al. [21] prediction of increasing mass-loss rate with increasing luminosity for a handful of Galactic RSGs. Similar figures exist in Gordon et al. [13], Meynet et al. [84] and others for Galactic and extragalactic RSGs (see Figure 9 below which illustrates a similar trend for total ejecta mass lost).
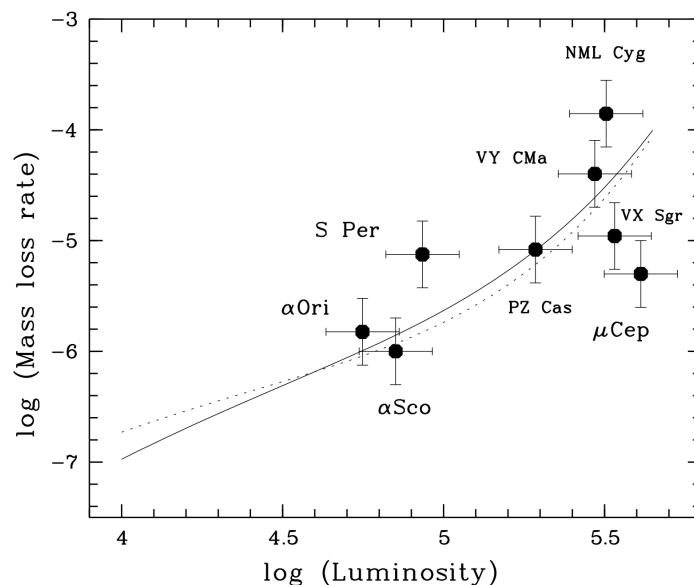

Figure 8. Mass-loss rates vs. luminosity for Galactic RSGs. The solid line represents the de Jager et al. [21] model for stellar $T_{\text{eff}} = 4000$ K and the dotted line for $T_{\text{eff}} = 3500$ K. Figure adapted from Reference [3].
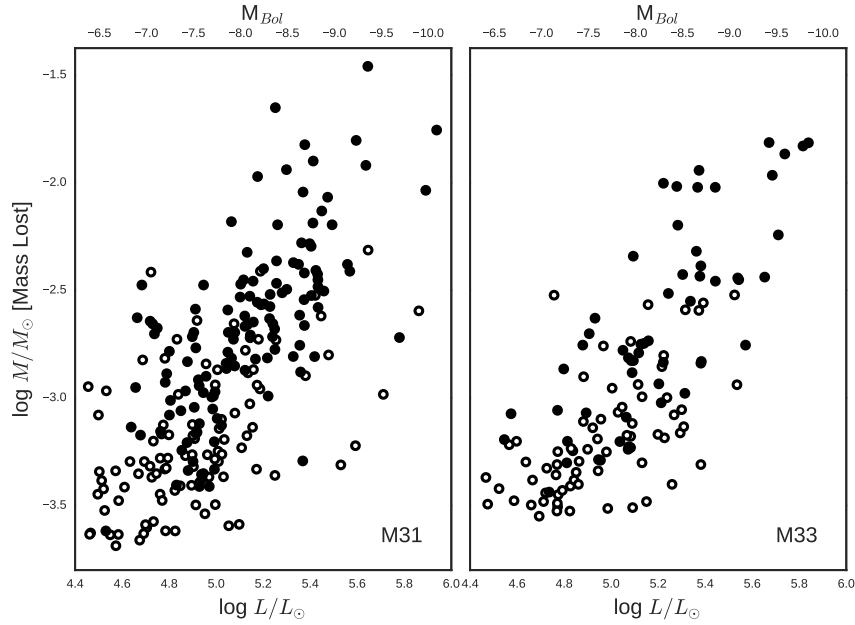
Figure 9. Bolometric luminosity vs. total mass lost based on dust measurements for RSG candidates in M31 and M33. Closed circles are those with clear evidence for mass loss in their SEDs. Open circles are the less certain mass losers. We note that the RSGs with higher luminosity tend to have lost more mass, consistent with the prescription of de Jager et al. [21] for mass loss in RSGs. Figure adapted from Reference [13].

The DUSTY radiative transfer code [25] is now often used to derive mass-loss rates or total ejected mass. DUSTY solves the radiative transfer equation for a spherically-symmetric dust distribution around a central source. Input parameters include the spectrum of the illuminating source, the optical properties and size distribution of the dust grains, the dust temperature at the inner boundary of the shell and a functional form for the radial profile of the dust density throughout the shell. The primary output is the resulting SED of the modeled system. This code has been recently been applied to different populations of RSGs and their ejecta to derive $\dot{M}$-luminosity relations from the IR SED fitting [24,56,86,87].

Shenoy et al. [56] and Gordon et al. [87] used DUSTY to generate radial profiles for a variety of model dust density profiles to test whether the mass-loss rates of the target RSGs are constant and smooth over time (e.g., $\rho_{\mathrm{dust}} \propto r^{-2}$) or if the circumstellar ejecta can be better modeled by one (or more) discrete, high-mass ejecta events. This methodology, however, requires high-resolution imaging both to trace the ejecta close to the central star and also to resolve the thermal emission above the PSF of the telescope/instrument used for the observations. These studies demonstrated that a spherically-symmetric shell model with constant mass loss over time does not adequately explain the morphology of the circumstellar ejecta in many yellow and red supergiants. In fact, variable mass loss over time is required to build up the multiple dust shells observed around several Galactic RSGs.

6.1. Mass-Loss Mechanisms and High Mass-Loss Events

Both ground and space-based high-resolution imaging and interferometry of evolved massive stars are transforming our view of mass loss and the mass-loss mechanism in evolved stars. The precise mass-loss mechanism for red supergiants is not fully understood. The leading processes have included radiation pressure on grains, pulsation and convection. The discovery of large-scale surface asymmetries or hot spots on the surfaces of red supergiants ([88–90] and more recently [91–93]), which vary on short timescales of months or years, supports the important role of convection and surface activity.

Pulsation and dust-driven winds have been successful at explaining mass loss in Miras and AGB stars, which are fundamental-mode pulsators. However, less variable RSGs with extended, low-density atmospheres are quite different environments than their lower-mass counterparts. Pulsation may be important for the YSGs, which are at the upper-luminosity limit of the Cepheid instability strip. For example, the light and velocity curves for ρ Cas [40] support a pulsational instability as the origin of its three brief, high mass-loss episodes. Yet, as discussed in Section 4, the peculiar M33 Var A's 45+ year high mass-loss episode [59], during which it resembled an M supergiant, required some high mass-loss mechanism lasting decades. Additionally, there exists significant dispersion in the measured mass-loss rates for stars of a given luminosity class. For example, Mauron and Josselin [3] compiled mass-loss rates for LMC RSGs from several data sets [17,94,95] to demonstrate that for stars around 10^5 L$_\odot$, a rather wide range of mass-loss rates between 10^{-6} and 10^{-4} M$_\odot$ yr^{-1} have been measured (see their Figure 5).

This dispersion may well be due to observational bias or different measurement techniques or may indeed be a manifestation of whatever physical mass-loss mechanism is at play. One approach to mitigate systematics in this mass-loss rate dispersion is to study individual RSG cluster populations. Beasor and Davies [86] compared RSGs within NGC 7419 and χ Per, whose stars are of similar ages, $\sim$14 Myr; [96,97]. With a focus on these coeval populations, the effects of age, metallicity and environment on $\dot{M}$ are removed and they find a tight correlation of mass-loss rate with luminosity.

Optical and near-IR imaging of the extreme OH/IR supergiant VY CMa and the post-RSG IRC +10420 (Section 4) have yielded surprising results about the circumstellar environments around massive stars. VY CMa has an extensive, highly structured nebula consisting of multiple knots and arcs ejected within the last 1000 years [47,53,98–100]. The numerous knots, arcs and loops visible in scattered light from the dust in their ejecta are structurally and kinematically distinct from the surrounding diffuse ejecta (see, for example, References [60,100]). These features were each ejected at different times over several hundred years, presumably by localized processes from different regions on the star. Estimates of the mass in some of the arcs and clumps in VY CMa's ejecta from surface photomety in the HST images and from the near-IR imaging of the southwest clump feature [101,102], yield minimum masses of 3–5$\times$10^{-3} M$_\odot$ implying short term, high mass-loss events. These discrete ejecta events hint at a very different ejecta mechanism than the slow, spherical shell paradigm. The presence of magnetic fields from Zeeman splitting and polarization of the OH/water masers has been detected in the circumstellar ejecta of VY CMa and other OH/IR supergiants such as VX Sgr, NML Cyg, and S Per [103–105]. These results suggest that enhanced surface convective activity (e.g.,in α Orionis; [92,93,106]) together with magnetic activity may be important for these high mass ejection events.

Recently, HST/STIS spectra revealed TiO and VO molecular emission discrete ejecta close to the central star in VY CMa [60]. These molecules, previously believed to form in low-density dusty CS shells, instead appear concentrated in small clumps and knots. Coupled with extremely strong K I emission (4 L$_\odot$ in just two narrow doublet lines; [60,98]), the emission features imply a dust-free environment between the knots and the star. These localized sources of atomic and molecular emission imply major gaps or holes in the star's envelope or outflow structure perhaps formed by large-scale surface activity.

7. Related Work

Two related fields of study not yet discussed are the effects of stellar pulsation and binarity in RSG/YSG stars. Stellar pulsations may serve as an effective observational discriminant between post-RSG stars and main-sequence OB-stars migrating towards the RSG branch for the first time. Saio et al. [82] modeled the pulsation periods of supergiants with the Geneva stellar evolution code and found that most non-radial pulsations are only excited after significant mass loss on the RSG branch. In particular, the models appear to predict the pulsation periods of the α Cygni variables, suggesting these stars are in a He-burning, post-RSG phase. Further, the models presented in that work and its follow-up [83] suggest that CNO surface abundances should be different in the two stellar

populations, owing to increased dredge up along the RSG branch. Convective cells and their effect on both surface abundance and pulsational properties remains largely unexplored on the observational side of stellar astrophysics for post-RSG stars but may well be a useful diagnostic for evolutionary state.

One final topic to consider is the role of binarity in massive star systems. More than 70% of O- and B-type stars have a binary companion [107,108] suggesting that their evolved counterparts—typically RSG+B binary pairs—should also be numerous. Recent observations by Neugent et al. [109] show that optical spectroscopy alone can be used to detect RSG+B star binaries and studying these systems prior to a SN explosion is critical, since Kochanek et al. [110] demonstrates that only ∼5% of SN remnants contain a surviving star plus remnant binary. Eldridge et al. [111] suggest that binary interactions may well be the cause of SN Type Ibc explosions, as the interaction strips much of the hydrogen from the stellar surface before the terminal explosion. However, the modeling from that work does not necessarily implicate the higher mass RSG/YSG pairs in the statistics for Type II-P progenitor systems. That said, earlier work by Eldridge et al. [5] suggest that enhanced mass transfer, colliding winds, gravitational distortion, and other binary interaction effects may indeed hasten an RSG towards core-collapse. The field of binary interactions is an entire genre of astrophysics which we cannot hope to summarize in this work but we note that binarity can significantly alter the HR diagram for high-mass/high-luminosity objects. A great summary of binarity and multiplicity in stellar systems as it relates to RSGs in particular can be found in Chapter 5 in Levesque [112].

Many of the luminous warm and cool hypergiants have extensive CS ejecta and evidence for high mass-loss events. The yellow hypergiants and many of the yellow supergiants are candidates for post red supergiant evolution. IRC +10420, Var A and the extreme red supergiant VY CMa may be the special cases that provide the clues to understanding evolution near the top of the HR Diagram. These stars represent short-lived, unstable states that signal the last stages in RSG evolution and the brief post-RSG transition as the star returns to warmer temperatures. This class of post-RSG stars with complex mass-loss histories may be the missing piece on the HR Diagram and the solution to the red supergiant problem.

Conflicts of Interest: The authors declare no conflict of interest.

Abbreviations

The following abbreviations are used in this manuscript:

2MASS	Two-Micron All Sky Survey
BSG	Blue Supergiant
CCSNe	Core-collapse supernovae
CMD	Color-magnitude diagram
CS	Circumstellar [ejecta]
HRD	Hertzsprung-Russell diagram
HST	Hubble Space Telescope
IR	Infrared
IRAC	Infrared Array Camera (Spitzer)
IRAS	Infrared Astronomical Satellite
LBV	Luminous Blue Variable
LGGS	Local Group Galaxy Survey
LMC	Large Magellanic Cloud

MIRAC   Mid-Infrared Array Camera (MMT)
PSF   Point spread function
RSG   Red Supergiant
SED   Spectral energy distribution
SN[e]   Supernova[e]
STIS   Space Telescope Imaging Spectrograph (HST)
WISE   Wide-field Infrared Survey Explorer
WR   Wolf-Rayet
YSG   Yellow Supergiant
ZAMS   Zero-age main-sequence

References

1. Humphreys, R.M.; Davidson, K. Studies of luminous stars in nearby galaxies. III—Comments on the evolution of the most massive stars in the Milky Way and the Large Magellanic Cloud. *Astrophys. J.* **1979**, *232*, 409–420, doi:10.1086/157301. [CrossRef]

2. Gehrz, R.D.; Woolf, N.J. Mass Loss from M Stars. *Astrophys. J.* **1971**, *165*, 285, doi:10.1086/150897. [CrossRef]

3. Mauron, N.; Josselin, E. The mass-loss rates of red supergiants and the de Jager prescription. *Astron. Astrophys.* **2011**, *526*, A156. [CrossRef]

4. Humphreys, R.M.; Davidson, K.; Grammer, S.; Kneeland, N.; Martin, J.C.; Weis, K.; Burggraf, B. Luminous and Variable Stars in M31 and M33. I. The Warm Hypergiants and Post-red Supergiant Evolution. *Astrophys. J.* **2013**, *773*, 46. [CrossRef]

5. Eldridge, J.J.; Izzard, R.G.; Tout, C.A. The effect of massive binaries on stellar populations and supernova progenitors. *Mon. Not. R. Astron. Soc.* **2008**, *384*, 1109–1118.[CrossRef]

6. Smartt, S.J.; Eldridge, J.J.; Crockett, R.M.; Maund, J.R. The death of massive stars—I. Observational constraints on the progenitors of Type II-P supernovae. *Mon. Not. R. Astron. Soc.* **2009**, *395*, 1409–1437. [CrossRef]

7. Smartt, S.J. Progenitors of Core-Collapse Supernovae. *Annu. Rev. Astron. Astrophys.* **2009**, *47*, 63–106. [CrossRef]

8. Li, W.; Leaman, J.; Chornock, R.; Filippenko, A.V.; Poznanski, D.; Ganeshalingam, M.; Wang, X.; Modjaz, M.; Jha, S.; Foley, R.J.; et al. Nearby supernova rates from the Lick Observatory Supernova Search—II. The observed luminosity functions and fractions of supernovae in a complete sample. *Mon. Not. R. Astron. Soc.* **2011**, *412*, 1441–1472. [CrossRef]

9. Levesque, E.M.; Massey, P.; Olsen, K.A.G.; Plez, B.; Josselin, E.; Maeder, A.; Meynet, G. The Effective Temperature Scale of Galactic Red Supergiants: Cool, but Not As Cool As We Thought. *Astrophys. J.* **2005**, *628*, 973–985. [CrossRef]

10. Levesque, E.M.; Massey, P.; Olsen, K.A.G.; Plez, B.; Meynet, G.; Maeder, A. The Effective Temperatures and Physical Properties of Magellanic Cloud Red Supergiants: The Effects of Metallicity. *Astrophys. J.* **2006**, *645*, 1102–1117. [CrossRef]

11. Massey, P.; Silva, D.R.; Levesque, E.M.; Plez, B.; Olsen, K.A.G.; Clayton, G.C.; Meynet, G.; Maeder, A. Red Supergiants in the Andromeda Galaxy (M31). *Astrophys. J.* **2009**, *703*, 420–440. [CrossRef]

12. Drout, M.R.; Massey, P.; Meynet, G. The Yellow and Red Supergiants of M33. *Astrophys. J.* **2012**, *750*, 97. [CrossRef]

13. Gordon, M.S.; Humphreys, R.M.; Jones, T.J. Luminous and Variable Stars in M31 and M33. III. The Yellow and Red Supergiants and Post-red Supergiant Evolution. *Astrophys. J.* **2016**, *825*, 50. doi: 10.3847/0004-637X/825/1/50. [CrossRef]

14. Meynet, G.; Maeder, A. Stellar evolution with rotation. X. Wolf-Rayet star populations at solar metallicity. *Astron. Astrophys.* **2003**, *404*, 975–990. [CrossRef]

15. Smith, N.; Li, W.; Filippenko, A.V.; Chornock, R. Observed fractions of core-collapse supernova types and initial masses of their single and binary progenitor stars. *Mon. Not. R. Astron. Soc.* **2011**, *412*, 1522–1538. [CrossRef]

16. Walmswell, J.J.; Eldridge, J.J. Circumstellar dust as a solution to the red supergiant supernova progenitor problem. *Mon. Not. R. Astron. Soc.* **2012**, *419*, 2054–2062. [CrossRef]

17.   van Loon, J.T.; Cioni, M.R.L.; Zijlstra, A.A.; Loup, C.   An empirical formula for the mass-loss rates of dust-enshrouded red supergiants and oxygen-rich Asymptotic Giant Branch stars. *Astron. Astrophys.* **2005**, *438*, 273–289. [CrossRef]

18.   Danchi, W.C.; Bester, M.; Degiacomi, C.G.; Greenhill, L.J.; Townes, C.H. Characteristics of dust shells around 13 late-type stars. *Astron. J.* **1994**, *107*, 1469–1513, doi:10.1086/116960. [CrossRef]

19.   Eggleton, P.P.   The evolution of low mass stars.   *Mon. Not. R. Astron. Soc.*   **1971**, *151*, 351, doi:10.1093/mnras/151.3.351. [CrossRef]

20.   Stancliffe, R.J.; Eldridge, J.J. Modelling the binary progenitor of Supernova 1993J. *Mon. Not. R. Astron. Soc.* **2009**, *396*, 1699–1708. [CrossRef]

21.   De Jager, C.; Nieuwenhuijzen, H.; van der Hucht, K.A. Mass loss rates in the Hertzsprung-Russell diagram. *Astron. Astrophys.* **1988**, *72*, 259–289.

22.   Vink, J.S.; de Koter, A.; Lamers, H.J.G.L.M. Mass-loss predictions for O and B stars as a function of metallicity. *Astron. Astrophys.* **2001**, *369*, 574–588. [CrossRef]

23.   Eldridge, J.J.; Tout, C.A.   The progenitors of core-collapse supernovae.   *Mon. Not. R. Astron. Soc.* **2004**, *353*, 87–97. [CrossRef]

24.   Beasor, E.R.; Davies, B. The evolution of red supergiants to supernova in NGC 2100. *Mon. Not. R. Astron. Soc.* **2016**, *463*, 1269–1283. [CrossRef]

25.   Ivezic, Z.; Nenkova, M.; Elitzur, M. *DUSTY: Radiation Transport in a Dusty Environment*; Astrophysics Source Code Library: Houghton, MI, USA, 1999.

26.   Kilpatrick, C.D.; Foley, R.J.   The dusty progenitor star of the Type II supernova 2017eaw.   *Mon. Not. R. Astron. Soc.* **2018**, *481*, 2536–2547. [CrossRef]

27.   Chevalier, R.A.; Fransson, C.   Supernova Interaction with a Circumstellar Medium.   In *Supernovae and Gamma-Ray Bursters*; Weiler, K., Ed.; Springer: Berlin, Germany, 2003; Volume 598, pp. 171–194. [CrossRef]

28.   Dwarkadas, V.V.; Gruszko, J.   What are published X-ray light curves telling us about young supernova expansion? *Mon. Not. R. Astron. Soc.* **2012**, *419*, 1515–1524. [CrossRef]

29.   Smartt, S.J. Observational Constraints on the Progenitors of Core-Collapse Supernovae: The Case for Missing High-Mass Stars. *PASA* **2015**, *32*, e016. [CrossRef]

30.   Kochanek, C.S.; Beacom, J.F.; Kistler, M.D.; Prieto, J.L.; Stanek, K.Z.; Thompson, T.A.; Yüksel, H. A Survey About Nothing: Monitoring a Million Supergiants for Failed Supernovae. *Astrophys. J.* **2008**, *684*, 1336–1342. [CrossRef]

31.   Ugliano, M.; Janka, H.T.; Marek, A.; Arcones, A.   Progenitor-explosion Connection and Remnant Birth Masses for Neutrino-driven Supernovae of Iron-core Progenitors. *Astrophys. J.* **2012**, *757*, 69. [CrossRef]

32.   Pejcha, O.; Thompson, T.A.   The Landscape of the Neutrino Mechanism of Core-collapse Supernovae: Neutron Star and Black Hole Mass Functions, Explosion Energies, and Nickel Yields. *Astrophys. J.* **2015**, *801*, 90. [CrossRef]

33.   Gerke, J.R.; Kochanek, C.S.; Stanek, K.Z. The search for failed supernovae with the Large Binocular Telescope: first candidates. *Mon. Not. R. Astron. Soc.* **2015**, *450*, 3289–3305. [CrossRef]

34.   Woosley, S.E.; Heger, A. Long Gamma-Ray Transients from Collapsars. *Astrophys. J.* **2012**, *752*, 32. [CrossRef]

35.   Lovegrove, E.; Woosley, S.E. Very Low Energy Supernovae from Neutrino Mass Loss. *Astrophys. J.* **2013**, *769*, 109. [CrossRef]

36.   Piro, A.L. Taking the "Un" out of "Unnovae". *Astrophys. J.* **2013**, *768*, L14. [CrossRef]

37.   Adams, S.M.; Kochanek, C.S.; Gerke, J.R.; Stanek, K.Z.; Dai, X. The search for failed supernovae with the Large Binocular Telescope: confirmation of a disappearing star. *Mon. Not. R. Astron. Soc.* **2017**, *468*, 4968–4981. [CrossRef]

38.   Humphreys, R.M. Comments on the Progenitor of NGC 6946-BH1. *Res. Notes Am. Astron. Soc.* **2019**, *3*, 164. [CrossRef]

39.   De Jager, C.; Nieuwenhuijzen, H. (Eds.) *Instabilities in Evolved Super- and Hypergiants*; Royal Netherlands Academy of Arts and Sciences: Amsterdam, The Netherlands, 1992.

40.   Lobel, A.; Dupree, A.K.; Stefanik, R.P.; Torres, G.; Israelian, G.; Morrison, N.; de Jager, C.; Nieuwenhuijzen, H.; Ilyin, I.; Musaev, F. High-Resolution Spectroscopy of the Yellow Hypergiant ρ Cassiopeiae from 1993 through the Outburst of 2000-2001. *Astrophys. J.* **2003**, *583*, 923–954. [CrossRef]

41. Nieuwenhuijzen, H.; De Jager, C.; Kolka, I.; Israelian, G.; Lobel, A.; Zsoldos, E.; Maeder, A.; Meynet, G. The hypergiant HR 8752 evolving through the yellow evolutionary void. *Astron. Astrophys.* **2012**, *546*, A105, doi:10.1051/0004-6361/201117166. [CrossRef]

42. Lobel, A.; de Jager, C.; Nieuwenhuijzen, H.; van Genderen, A.M.; Oudmaijer, R. Yellow Hypergiants: A Comparative Study of HR 5171A, Rho Cas, and HR 8752. *EAS Publ. Ser.* **2015**, *71*, 279–280, doi:10.1051/eas/1571062. [CrossRef]

43. Chesneau, O.; Meilland, A.; Chapellier, E.; Millour, F.; van Genderen, A.M.; Nazé, Y.; Smith, N.; Spang, A.; Smoker, J.V.; Dessart, L.; et al. The yellow hypergiant HR 5171 A: Resolving a massive interacting binary in the common envelope phase. *Astron. Astrophys.* **2014**, *563*, A71. [CrossRef]

44. De Jager, C. The yellow hypergiants. *Astron. Astrophys.* **1998**, *8*, 145–180, doi:10.1007/s001590050009. [CrossRef]

45. Humphreys, R.M.; Strecker, D.W.; Murdock, T.L.; Low, F.J. IRC+10420—Another Eta Carinae? *Astrophys. J.* **1973**, *179*, L49, doi:10.1086/181114. [CrossRef]

46. Giguere, P.T.; Woolf, N.J.; Webber, J.C. IRC +10 420—A hot supergiant maser. *Astrophys. J.* **1976**, *207*, L195–L198, doi:10.1086/182211. [CrossRef]

47. Humphreys, R.M.; Smith, N.; Davidson, K.; Jones, T.J.; Gehrz, R.T.; Mason, C.G.; Hayward, T.L.; Houck, J.R.; Krautter, J. HST and Infrared Images of the Circumstellar Environment of the Cool Hypergiant IRC + 10420. *Astron. J.* **1997**, *114*, 2778, doi:10.1086/118686. [CrossRef]

48. Humphreys, R.M.; Davidson, K.; Smith, N. Crossing the Yellow Void: Spatially Resolved Spectroscopy of the Post-Red Supergiant IRC +10420 and Its Circumstellar Ejecta. *Astron. J.* **2002**, *124*, 1026–1044. doi: 10.1086/341380. [CrossRef]

49. Oudmaijer, R.D.; Groenewegen, M.A.T.; Matthews, H.E.; Blommaert, J.A.D.L.; Sahu, K.C. The spectral energy distribution and mass-loss history of IRC+10420. *Mon. Not. R. Astron. Soc.* **1996**, *280*, 1062–1070, doi:10.1093/mnras/280.4.1062. [CrossRef]

50. Jones, T.J.; Humphreys, R.M.; Gehrz, R.D.; Lawrence, G.F.; Zickgraf, F.J.; Moseley, H.; Casey, S.; Glaccum, W.J.; Koch, C.J.; Pina, R.; et al. IRC +10420—A cool hypergiant near the top of the H-R diagram. *Astrophys. J.* **1993**, *411*, 323–335, doi:10.1086/172832. [CrossRef]

51. Oudmaijer, R.D. High resolution spectroscopy of the post-red supergiant IRC+10420. I. The data. *Astron. Astrophys.s* **1998**, *129*, 541–552, doi:10.1051/aas:1998404. [CrossRef]

52. Klochkova, V.G.; Chentsov, E.L.; Miroshnichenko, A.S.; Panchuk, V.E.; Yushkin, M.V. High-resolution optical spectroscopy of the yellow hypergiant V1302 Aql (=IRC+10420) in 2001-2014. *Mon. Not. R. Astron. Soc.* **2016**, *459*, 4183–4190. doi: 10.1093/mnras/stw902. [CrossRef]

53. Tiffany, C.; Humphreys, R.M.; Jones, T.J.; Davidson, K. The Morphology of IRC+10420's Circumstellar Ejecta. *Astron. J.* **2010**, *140*, 339–349. doi: 10.1088/0004-6256/140/2/339. [CrossRef]

54. Shenoy, D.P.; Jones, T.J.; Packham, C.; Lopez-Rodriguez, E. Probing Hypergiant Mass Loss with Adaptive Optics Imaging and Polarimetry in the Infrared: MMT-Pol and LMIRCam Observations of IRC +10420 and VY Canis Majoris. *Astron. J.* **2015**, *150*, 15. doi: 10.1088/0004-6256/150/1/15. [CrossRef]

55. De Wit, W.J.; Oudmaijer, R.D.; Fujiyoshi, T.; Hoare, M.G.; Honda, M.; Kataza, H.; Miyata, T.; Okamoto, Y.K.; Onaka, T.; Sako, S.; et al. A Red Supergiant Nebula at 25 μm: Arcsecond-Scale Mass-Loss Asymmetries of μ Cephei. *Astrophys. J.* **2008**, *685*, L75. doi: 10.1086/592384. [CrossRef]

56. Shenoy, D.; Humphreys, R.M.; Jones, T.J.; Marengo, M.; Gehrz, R.D.; Helton, L.A.; Hoffmann, W.F.; Skemer, A.J.; Hinz, P.M. Searching for Cool Dust in the Mid-to-far Infrared: The Mass-loss Histories of the Hypergiants μ Cep, VY CMa, IRC+10420, and ρ Cas. *Astron. J.* **2016**, *151*, 51. doi: 10.3847/0004-6256/151/3/51. [CrossRef]

57. Hubble, E.; Sandage, A. The Brightest Variable Stars in Extragalactic Nebulae. I. M31 and M33. *Astrophys. J.* **1953**, *118*, 353, doi:10.1086/145764. [CrossRef]

58. Humphreys, R.M.; Jones, T.J.; Gehrz, R.D. The enigmatic object variable A in M33. *Astron. J.* **1987**, *94*, 315–323, doi:10.1086/114473. [CrossRef]

59. Humphreys, R.M.; Jones, T.J.; Polomski, E.; Koppelman, M.; Helton, A.; McQuinn, K.; Gehrz, R.D.; Woodward, C.E.; Wagner, R.M.; Gordon, K.; et al. M33's Variable A: A Hypergiant Star More Than 35 YEARS in Eruption. *Astron. J.* **2006**, *131*, 2105–2113. doi: 10.1086/500811. [CrossRef]

60. Humphreys, R.M.; Ziurys, L.M.; Bernal, J.J.; Gordon, M.S.; Helton, L.A.; Ishibashi, K.; Jones, T.J.; Richards, A.M.S.; Vlemmings, W. The Unexpected Spectrum of the Innermost Ejecta of the Red Hypergiant VY CMa. *Astrophys. J.* **2019**, *874*, L26. doi: 10.3847/2041-8213/ab11e5. [CrossRef]

61. Drout, M.R.; Massey, P.; Meynet, G.; Tokarz, S.; Caldwell, N. Yellow Supergiants in the Andromeda Galaxy (M31). *Astrophys. J.* **2009**, *703*, 441–460. doi: 10.1088/0004-637X/703/1/441. [CrossRef]

62. Massey, P.; Olsen, K.A.G.; Hodge, P.W.; Strong, S.B.; Jacoby, G.H.; Schlingman, W.; Smith, R.C. A Survey of Local Group Galaxies Currently Forming Stars. I. UBVRI Photometry of Stars in M31 and M33. *Astron. J.* **2006**, *131*, 2478–2496. doi: 10.1086/503256. [CrossRef]

63. Kourniotis, M.; Bonanos, A.Z.; Yuan, W.; Macri, L.M.; Garcia-Alvarez, D.; Lee, C.H. Monitoring luminous yellow massive stars in M 33: New yellow hypergiant candidates. *Astron. Astrophys.* **2017**, *601*, A76. doi: 10.1051/0004-6361/201629146. [CrossRef]

64. Humphreys, R.M.; Sandage, A. On the stellar content and structure of the spiral Galaxy M33. *Astrophys. J.* **1980**, *44*, 319–381, doi:10.1086/190696. [CrossRef]

65. Massey, P.; Olsen, K.A.G.; Hodge, P.W.; Jacoby, G.H.; McNeill, R.T.; Smith, R.C.; Strong, S.B. A Survey of Local Group Galaxies Currently Forming Stars. II. UBVRI Photometry of Stars in Seven Dwarfs and a Comparison of the Entire Sample. *Astron. J.* **2007**, *133*, 2393–2417. doi: 10.1086/513319. [CrossRef]

66. Bahcall, J.N.; Soneira, R.M. The universe at faint magnitudes. I—Models for the galaxy and the predicted star counts. *Astrophys. J.s* **1980**, *44*, 73–110, doi:10.1086/190685. [CrossRef]

67. Massey, P.; Neugent, K.F.; Smart, B.M. A Spectroscopic Survey of Massive Stars in M31 and M33. *Astron. J.* **2016**, *152*, 62. doi: 10.3847/0004-6256/152/3/62. [CrossRef]

68. Robin, A.C.; Reylé, C.; Derrière, S.; Picaud, S. A synthetic view on structure and evolution of the Milky Way. *Astron. Astrophys.* **2003**, *409*, 523–540, doi:10.1051/0004-6361:20031117. [CrossRef]

69. Massey, P. Evolved Massive Stars in the Local Group. I. Identification of Red Supergiants in NGC 6822, M31, and M33. *Astrophys. J.* **1998**, *501*, 153–174, doi:10.1086/305818. [CrossRef]

70. Bonanos, A.Z.; Massa, D.L.; Sewilo, M.; Lennon, D.J.; Panagia, N.; Smith, L.J.; Meixner, M.; Babler, B.L.; Bracker, S.; Meade, M.R.; et al. Spitzer SAGE Infrared Photometry of Massive Stars in the Large Magellanic Cloud. *Astron. J.* **2009**, *138*, 1003–1021. doi: 10.1088/0004-6256/138/4/1003. [CrossRef]

71. Bonanos, A.Z.; Lennon, D.J.; Köhlinger, F.; van Loon, J.T.; Massa, D.L.; Sewilo, M.; Evans, C.J.; Panagia, N.; Babler, B.L.; Block, M.; et al. Spitzer SAGE-SMC Infrared Photometry of Massive Stars in the Small Magellanic Cloud. *Astron. J.* **2010**, *140*, 416–429. doi: 10.1088/0004-6256/140/2/416. [CrossRef]

72. Woolf, N.J.; Ney, E.P. Circumstellar Infrared Emission from Cool Stars. *Astrophys. J.* **1969**, *155*, L181, doi:10.1086/180331. [CrossRef]

73. Treffers, R.; Cohen, M. High-resolution spectra of cool stars in the 10- and 20-micron regions. *Astrophys. J.* **1974**, *188*, 545–552, doi:10.1086/152746. [CrossRef]

74. Kurucz, R.L. Model atmospheres for G, F, A, B, and O stars. *Astrophys. J.* **1979**, *40*, 1–340, doi:10.1086/190589. [CrossRef]

75. Howarth, I.D. New limb-darkening coefficients and synthetic photometry for model-atmosphere grids at Galactic, LMC and SMC abundances. *Mon. Not. R. Astron. Soc.* **2011**, *413*, 1515–1523. doi: 10.1111/j.1365-2966.2011.18122.x. [CrossRef]

76. McQuinn, K.B.W.; Woodward, C.E.; Willner, S.P.; Polomski, E.F.; Gehrz, R.D.; Humphreys, R.M.; van Loon, J.T.; Ashby, M.L.N.; Eicher, K.; Fazio, G.G. The M33 Variable Star Population Revealed by Spitzer. *Astrophys. J.* **2007**, *664*, 850–861. doi: 10.1086/519068. [CrossRef]

77. Mould, J.; Barmby, P.; Gordon, K.; Willner, S.P.; Ashby, M.L.N.; Gehrz, R.D.; Humphreys, R.; Woodward, C.E. A Point-Source Survey of M31 with the Spitzer Space Telescope. *Astrophys. J.* **2008**, *687*, 230–241. doi: 10.1086/591844. [CrossRef]

78. Khan, R.; Stanek, K.Z.; Kochanek, C.S.; Sonneborn, G. Spitzer Point-source Catalogs of ∽300,000 Stars in Seven Nearby Galaxies. *Astrophys. J.* **2015**, *219*, 42. doi: 10.1088/0067-0049/219/2/42. [CrossRef]

79. Khan, R.; Kochanek, C.S.; Stanek, K.Z.; Gerke, J. Finding η Car Analogs in Nearby Galaxies Using Spitzer. II. Identification of An Emerging Class of Extragalactic Self-Obscured Stars. *Astrophys. J.* **2015**, *799*, 187. doi: 10.1088/0004-637X/799/2/187. [CrossRef]

80. Ekström, S.; Georgy, C.; Eggenberger, P.; Meynet, G.; Mowlavi, N.; Wyttenbach, A.; Granada, A.; Decressin, T.; Hirschi, R.; Frischknecht, U.; et al. Grids of stellar models with rotation - I. Models from 0.8 to 120 M solar metallicity (Z = 0.014). *Astron. Astrophys.* **2012**, *537*, A146. doi: 10.1051/0004-6361/201117751. [CrossRef]

81. Meynet, G.; Kudritzki, R.P.; Georgy, C. The flux-weighted gravity-luminosity relationship of blue supergiant stars as a constraint for stellar evolution. *Astron. Astrophys.* **2015**, *581*, A36. doi: 10.1051/0004-6361/201526035. [CrossRef]

82. Saio, H.; Georgy, C.; Meynet, G. Evolution of blue supergiants and α Cygni variables: Puzzling CNO surface abundances. *Mon. Not. R. Astron. Soc.* **2013**, *433*, 1246–1257. doi: 10.1093/mnras/stt796. [CrossRef]

83. Georgy, C.; Saio, H.; Meynet, G. The puzzle of the CNO abundances of α Cygni variables resolved by the Ledoux criterion. *Mon. Not. R. Astron. Soc.* **2014**, *439*, L6–L10. doi: 10.1093/mnrasl/slt165. [CrossRef]

84. Meynet, G.; Chomienne, V.; Ekström, S.; Georgy, C.; Granada, A.; Groh, J.; Maeder, A.; Eggenberger, P.; Levesque, E.; Massey, P. Impact of mass-loss on the evolution and pre-supernova properties of red supergiants. *Astron. Astrophys.* **2015**, *575*, A60. doi: 10.1051/0004-6361/201424671. [CrossRef]

85. Kourniotis, M.; Kraus, M.; Arias, M.L.; Cidale, L.; Torres, A.F. On the evolutionary state of massive stars in transition phases in M33. *Mon. Not. R. Astron. Soc.* **2018**, *480*, 3706–3717. doi: 10.1093/mnras/sty2087. [CrossRef]

86. Beasor, E.R.; Davies, B. The evolution of red supergiant mass-loss rates. *Mon. Not. R. Astron. Soc.* **2018**, *475*, 55–62. doi: 10.1093/mnras/stx3174. [CrossRef]

87. Gordon, M.S.; Humphreys, R.M.; Jones, T.J.; Shenoy, D.; Gehrz, R.D.; Helton, L.A.; Marengo, M.; Hinz, P.M.; Hoffmann, W.F. Searching for Cool Dust. II. Infrared Imaging of The OH/IR Supergiants, NML Cyg, VX Sgr, S Per, and the Normal Red Supergiants RS Per and T Per. *Astron. J.* **2018**, *155*, 212. doi: 10.3847/1538-3881/aab961. [CrossRef]

88. Gilliland, R.L.; Dupree, A.K. First Image of the Surface of a Star with the Hubble Space Telescope. *Astrophys. J.l* **1996**, *463*, L29, doi:10.1086/310043. [CrossRef]

89. Tuthill, P.G.; Haniff, C.A.; Baldwin, J.E. Hotspots on late-type supergiants. *Mon. Not. R. Astron. Soc.* **1997**, *285*, 529–539, doi:10.1093/mnras/285.3.529. [CrossRef]

90. Monnier, J.D.; Millan-Gabet, R.; Tuthill, P.G.; Traub, W.A.; Carleton, N.P.; Coudé du Foresto, V.; Danchi, W.C.; Lacasse, M.G.; Morel, S.; Perrin, G.; et al. High-Resolution Imaging of Dust Shells by Using Keck Aperture Masking and the IOTA Interferometer. *Astrophys. J.* **2004**, *605*, 436–461. doi: 10.1086/382218. [CrossRef]

91. Montargès, M.; Norris, R.; Chiavassa, A.; Tessore, B.; Lèbre, A.; Baron, F. The convective photosphere of the red supergiant CE Tauri. I. VLTI/PIONIER H-band interferometric imaging. *Astron. Astrophys.* **2018**, *614*, A12. doi: 10.1051/0004-6361/201731471. [CrossRef]

92. Nance, S.; Sullivan, J.M.; Diaz, M.; Wheeler, J.C. The Betelgeuse Project II: asteroseismology. *Mon. Not. R. Astron. Soc.* **2018**, *479*, 251–261. doi: 10.1093/mnras/sty1418. [CrossRef]

93. López Ariste, A.; Mathias, P.; Tessore, B.; Lèbre, A.; Aurière, M.; Petit, P.; Ikhenache, N.; Josselin, E.; Morin, J.; Montargès, M. Convective cells in Betelgeuse: imaging through spectropolarimetry. *Astron. Astrophys.* **2018**, *620*, A199. doi: 10.1051/0004-6361/201834178. [CrossRef]

94. Reid, N.; Tinney, C.; Mould, J. Luminous asymptotic giant branch stars in the Large Magellanic Cloud. *Astrophys. J.* **1990**, *348*, 98–119, doi:10.1086/168217. [CrossRef]

95. Groenewegen, M.A.T.; Sloan, G.C.; Soszyński, I.; Petersen, E.A. Luminosities and mass-loss rates of SMC and LMC AGB stars and red supergiants. *Astron. Astrophys.* **2009**, *506*, 1277–1296. doi: 10.1051/0004-6361/200912678. [CrossRef]

96. Currie, T.; Hernandez, J.; Irwin, J.; Kenyon, S.J.; Tokarz, S.; Balog, Z.; Bragg, A.; Berlind, P.; Calkins, M. The Stellar Population of h and χ Persei: Cluster Properties, Membership, and the Intrinsic Colors and Temperatures of Stars. *Astrophys. J.* **2010**, *186*, 191–221. doi: 10.1088/0067-0049/186/2/191. [CrossRef]

97. Marco, A.; Negueruela, I. NGC 7419 as a template for red supergiant clusters. *Astron. Astrophys.* **2013**, *552*, A92. doi: 10.1051/0004-6361/201220750. [CrossRef]

98. Humphreys, R.M.; Davidson, K.; Ruch, G.; Wallerstein, G. High-Resolution, Long-Slit Spectroscopy of VY Canis Majoris: The Evidence for Localized High Mass Loss Events. *Astron. J.* **2005**, *129*, 492–510. doi: 10.1086/426565. [CrossRef]

99. Humphreys, R.M.; Helton, L.A.; Jones, T.J. The Three-Dimensional Morphology of VY Canis Majoris. I. The Kinematics of the Ejecta. *Astron. J.* **2007**, *133*, 2716–2729. doi: 10.1086/517609. [CrossRef]

100. Smith, N.; Humphreys, R.M.; Davidson, K.; Gehrz, R.D.; Schuster, M.T.; Krautter, J. The Asymmetric Nebula Surrounding the Extreme Red Supergiant VY Canis Majoris. *Astron. J.* **2001**, *121*, 1111–1125, doi:10.1086/318748. [CrossRef]

101. Shenoy, D.P.; Jones, T.J.; Humphreys, R.M.; Marengo, M.; Leisenring, J.M.; Nelson, M.J.; Wilson, J.C.; Skrutskie, M.F.; Hinz, P.M.; Hoffmann, W.F.; et al. Adaptive Optics Imaging of VY Canis Majoris at 2-5 μm with LBT/LMIRCam. *Astron. J.* **2013**, *146*, 90. doi: 10.1088/0004-6256/146/4/90. [CrossRef]

102. Gordon, M.S.; Jones, T.J.; Humphreys, R.M.; Ertel, S.; Hinz, P.M.; Hoffmann, W.F.; Stone, J.; Spalding, E.; Vaz, A. Thermal Emission in the Southwest Clump of VY CMa. *Astron. J.* **2019**, *157*, 57. doi: 10.3847/1538-3881/aaf5cb. [CrossRef]

103. Vlemmings, W.H.T.; Diamond, P.J.; van Langevelde, H.J. Circular polarization of water masers in the circumstellar envelopes of late type stars. *Astron. Astrophys.* **2002**, *394*, 589–602. doi: 10.1051/0004-6361:20021166. [CrossRef]

104. Vlemmings, W.H.T.; van Langevelde, H.J.; Diamond, P.J.; Habing, H.J.; Schilizzi, R.T. VLBI astrometry of circumstellar OH masers: Proper motions and parallaxes of four AGB stars. *Astron. Astrophys.* **2003**, *407*, 213–224. doi: 10.1051/0004-6361:20030766. [CrossRef]

105. Vlemmings, W.H.T.; van Langevelde, H.J.; Diamond, P.J. The magnetic field around late-type stars revealed by the circumstellar H_2O masers. *Astron. Astrophys.* **2005**, *434*, 1029–1038. doi: 10.1051/0004-6361:20042488. [CrossRef]

106. Kervella, P.; Lagadec, E.; Montargès, M.; Ridgway, S.T.; Chiavassa, A.; Haubois, X.; Schmid, H.M.; Langlois, M.; Gallenne, A.; Perrin, G. The close circumstellar environment of Betelgeuse. III. SPHERE/ZIMPOL imaging polarimetry in the visible. *Astron. Astrophys.* **2016**, *585*, A28. doi: 10.1051/0004-6361/201527134. [CrossRef]

107. Gies, D.R. Binaries in Massive Star Formation. In *Massive Star Formation: Observations Confront Theory*; ASP Conference Series; Beuther, H., Linz, H., Henning, T., Eds.; Astronomical Society of the Pacific: San Francisco, CA, USA, 2008; Volume 387, p. 93.

108. Sana, H.; de Mink, S.E.; de Koter, A.; Langer, N.; Evans, C.J.; Gieles, M.; Gosset, E.; Izzard, R.G.; Le Bouquin, J.B.; Schneider, F.R.N. Binary Interaction Dominates the Evolution of Massive Stars. *Science* **2012**, *337*, 444. doi: 10.1126/science.1223344. [CrossRef]

109. Neugent, K.F.; Levesque, E.M.; Massey, P. Binary Red Supergiants: A New Method for Detecting B-type Companions. *Astron. J.* **2018**, *156*, 225. doi: 10.3847/1538-3881/aae4e0. [CrossRef]

110. Kochanek, C.S.; Auchettl, K.; Belczynski, K. Stellar binaries that survive supernovae. *Mon. Not. R. Astron. Soc.* **2019**, *485*, 5394–5410. doi: 10.1093/mnras/stz717. [CrossRef]

111. Eldridge, J.J.; Fraser, M.; Smartt, S.J.; Maund, J.R.; Crockett, R.M. The death of massive stars—II. Observational constraints on the progenitors of Type Ibc supernovae. *Mon. Not. R. Astron. Soc.* **2013**, *436*, 774–795. doi: 10.1093/mnras/stt1612. [CrossRef]

112. Levesque, E.M. *Astrophysics of Red Supergiants*; IOP Publishing: Bristol, UK, 2017, doi:10.1088/978-0-7503-1329-2. [CrossRef]